Article

Accurate Flow Regime Classification and Void Fraction Measurement in Two-Phase Flowmeters Using Frequency-Domain Feature Extraction and Neural Networks

Siavash Hosseini [1], Abdullah M. Iliyasu [2,3,4,*], Thangarajah Akilan [1], Ahmed S. Salama [5], Ehsan Eftekhari-Zadeh [6,7,8,*] and Kaoru Hirota [3,9]

1 Department of Software Engineering, Lakehead University, Thunder Bay, ON P7B 5E1, Canada; shossei4@lakeheadu.ca (S.H.); takilan@lakeheadu.ca (T.A.)
2 Electrical Engineering Department, College of Engineering, Prince Sattam Bin Abdulaziz University, Al-Kharj 11942, Saudi Arabia
3 School of Computing, Tokyo Institute of Technology, Yokohama 226-8502, Japan; hirota@bit.edu.cn
4 School of Computer Science and Technology, Changchun University of Science and Technology, Changchun 130022, China
5 Electrical Engineering Department, Faculty of Engineering and Technology, Future University in Egypt, New Cairo 11835, Egypt; a.salama@fue.edu.eg
6 Institute of Optics and Quantum Electronics, Friedrich Schiller University Jena, Max-Wien-Platz 1, 07743 Jena, Germany
7 Abbe Center of Photonics, Friedrich Schiller University Jena, Albert Einstein Straße 6, 07745 Jena, Germany
8 Helmholtz Institute Jena, Fröbelstieg 3, 07743 Jena, Germany
9 School of Automation, Beijing Institute of Technology, Beijing 100081, China
* Correspondence: a.iliyasu@psau.edu.sa (A.M.I.); e.eftekharizadeh@uni-jena.de (E.E.-Z.)

Abstract: Two-phase flow is very important in many areas of science, engineering, and industry. Two-phase flow comprising gas and liquid phases is a common occurrence in oil and gas related industries. This study considers three flow regimes, including homogeneous, annular, and stratified regimes ranging from 5–90% of void fractions simulated via the Mont Carlo N-Particle (MCNP) Code. In the proposed model, two NaI detectors were used for recording the emitted photons of a cesium 137 source that pass through the pipe. Following that, fast Fourier transform (FFT), which aims to transfer recorded signals to frequency domain, was adopted. By analyzing signals in the frequency domain, it is possible to extract some hidden features that are not visible in the time domain analysis. Four distinctive features of registered signals, including average value, the amplitude of dominant frequency, standard deviation (STD), and skewness were extracted. These features were compared to each other to determine the best feature that can offer the best separation. Furthermore, artificial neural network (ANN) was utilized to increase the efficiency of two-phase flowmeters. Additionally, two multi-layer perceptron (MLP) neural networks were adopted for classifying the considered regimes and estimating the volumetric percentages. Applying the proposed model, the outlined flow regimes were accurately classified, resulting in volumetric percentages with a low root mean square error (RMSE) of 1.1%.

Keywords: artificial intelligence; two-phase flows; feature extraction; flow regimes; neural network; petroleum industry

1. Introduction

Nowadays, analyzing the flow regimes and volumetric percentages of multiphase flows is a significant and notable topic in many industries [1–3]. Liquids and gases are the most important elements in oil and gas storage. For better comprehension as to whether the drilling process is sensible or not, it is essential to measure each parameter [4]. Also, the separation procedure will be better developed, with adequate information about regime

types and volumes of each phase. In this regard, different methods have been studied for determining the mentioned parameters. According to former studies, gamma-ray attenuation technique was the most accurate method [1]. Abro and his colleagues investigated the efficiency of single- and multi-beam gamma-ray densitometry to estimate the volumetric percentages in two-phase flows consisting of gases and liquids [5]. According to their acquired results, the multi-beam gamma ray method was more accurate than the single-beam technique. Jing and co-workers investigated dual modality densitometry to classify the flow regimes in a vertical pipe [6]. In 2014, three flow regimes (see in Figure 1) (homogeneous, annular, and stratified) were simulated via MCNP code [4]. One ^{137}Cs source, one transmitted, and scattered detector were utilized as the proposed structure. For classifying the flow regimes and predicting volumetric percentages, three attributes of signals were extracted and used as the ANN inputs. Faghihi et al. studied stratified, homogeneous, and annular regimes in a pipe with vertical position for 3 different flow regimes [7]. Nazemi et al. investigated the gamma-ray attenuation technique in annular, bubbly, and stratified flow regimes in a two-phase flow structure. In this article, volume fraction was determined independent of regime type [8]. Two transmitted detectors were applied for registering the transmitted photons. In this situation, void fraction percentages were calculated using the MLP neural network. Nazemi et al. improved the accuracy of estimation by applying two features of registered signals in a Radial Basis Function (RBF) neural network for determining void fraction. By using the proposed method, the percentages of volume fraction were determined to be autonomous of density alterations in the liquid phase of the stratified regime [9]. Utilizing fewer detectors in structure is a matter of key importance in industries; not only does it lessen expenditures, but it also makes it easier to work with these systems. Roshani and co-workers analyzed a simple setup with single NaI detector, as well as a Co^{60} source, but they found that it was impossible to classify all the flow regimes using one detector in the structure, and only two of the regimes were identified [2]. Different features in the frequency domain were presented by Hanus and co-workers in order to identify the flow regimes in a dynamic condition [10]. In this work, three various structures of two-phase flows (air-water), including plug flow, bubble flow, and transitional plug-bubble flow were studied. Salgado et al. have several works which aimed to distinguish flow regimes and determine void fraction using ANNs [11–14]. Sattari et al. carried out research work by taking advantage of time-domain feature extraction for regime classification and void fraction prediction. By adopting time-domain techniques, volumetric percentages were estimated with an RMSE of 5.32 [15].
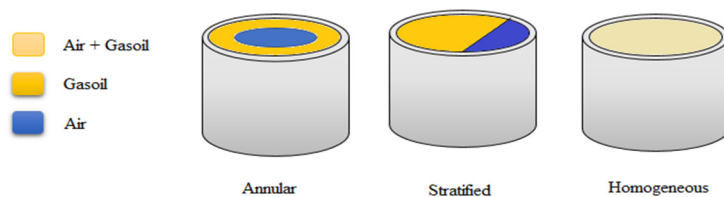

Figure 1. The flow regimes considered in the study.

In recent years, many researchers have put a great deal of effort into oil and gas fields for flow regime identification and void fraction measurement by utilizing different methods such as GMDH and wavelet feature extraction [16–18].

2. Simulation Procedure

The data collection process in this work includes two separated stages. Firstly, three principal regimes, including homogeneous, annular, and stratified were simulated using MCNP code. Simulations were accomplished for 5–90% void fraction. Gasoil and air were considered as the liquid and gas phases, respectively. A ^{137}Cs source and two NaI detectors were utilized in order to register photons that passed through the pipe with an inner diameter of 95 mm and a thickness of 2.5 mm.

Secondly, for evaluating the accuracy of the simulated structure (see in Figure 2) in MCNP code, simulated geometry was assessed for validity with multiple experiments in previous work [1]. The comparison between experimental and simulated data in the annular regime for first and second transmission detectors is shown in Figure 3. The maximum Relative Difference (RD) between experimental data and simulation data is 2.9%, which shows the good agreement between experimental and simulation results. Different stages of this work can be found in Figure 4.
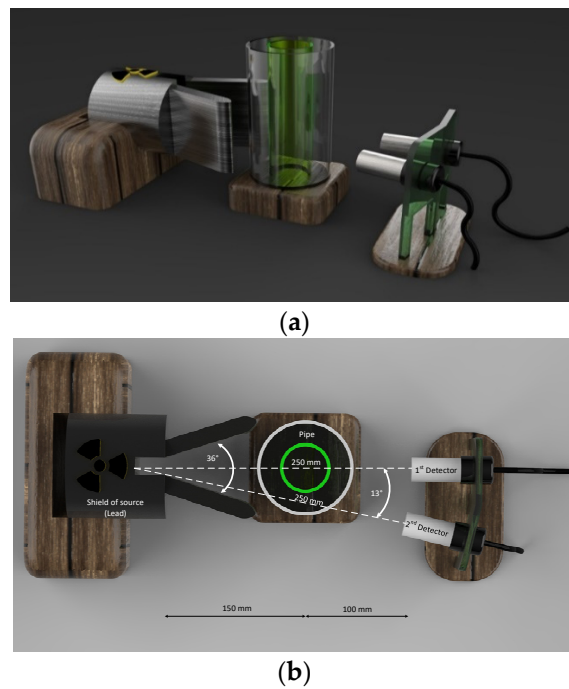

(**a**)

(**b**)

Figure 2. The structure of a simulated setup using MCNP: (**a**) 3D view, (**b**) View from above.
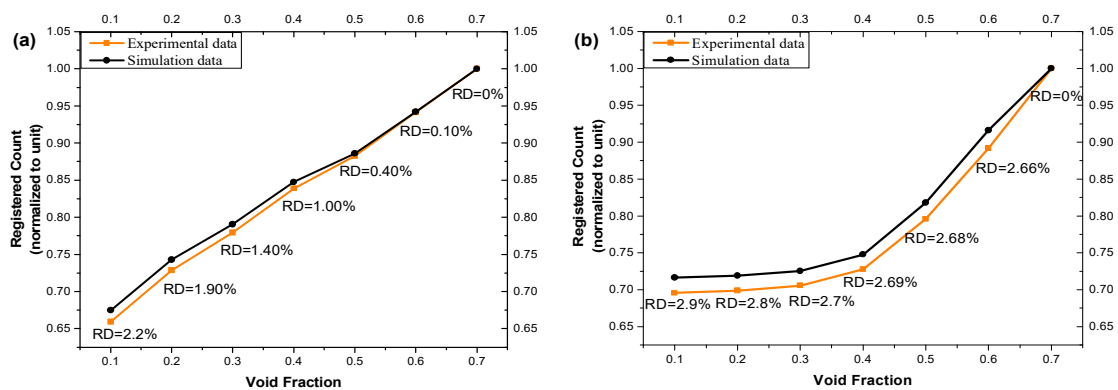

Figure 3. A comparison of experimental and simulation data in an annular regime for responses of (**a**) first transmission detector; (**b**) second transmission detector.
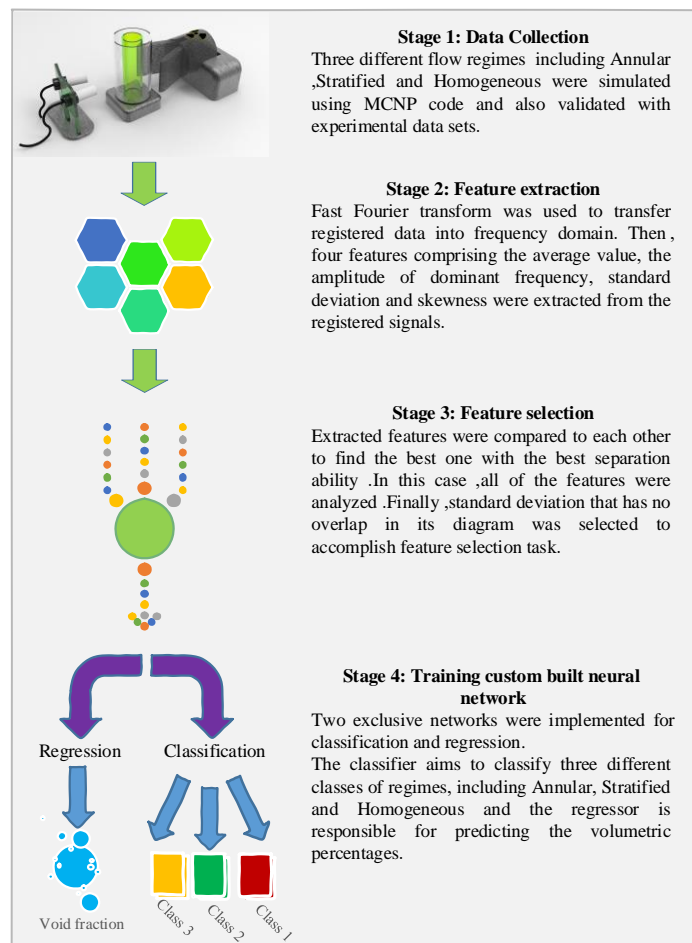
Figure 4. An outline of the proposed model.

3. Feature Extraction

Registered photon energy spectra for the 3 flow regimes (void fraction = 5%) are shown in Figure 5.
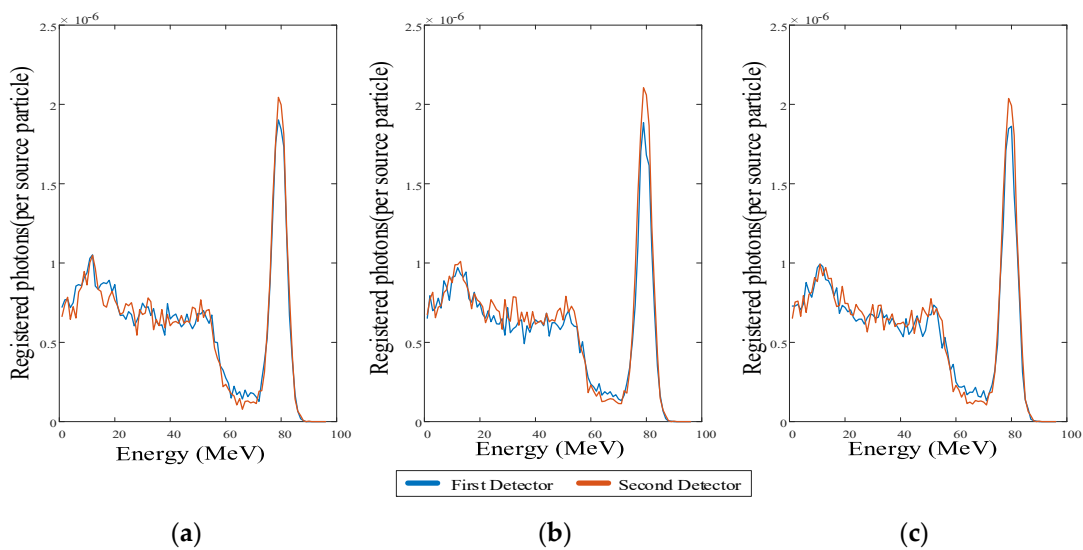

Figure 5. The registered photon energy spectra in the first and second detectors (void fraction = 5%): (**a**) annular, (**b**) homogenous, and (**c**) stratified.

In this study, after transforming recorded signals into frequency domain via fast Fourier transform, several features were extracted. Adopted features are as follows: average, the amplitude of dominant frequency, standard deviation (STD), and skewness. These are the foremost features in the feature extraction field, which have been used in dozens of studies [19].

The average value, standard deviation, and skewness are shown in Equations (1)–(3), respectively:

$$m = \frac{1}{N} \sum_{n=1}^{N} x[n] \tag{1}$$

$$\sigma = \sqrt{\frac{1}{N-1} \sum_{n=1}^{N} (x[n] - m)^2} \tag{2}$$

$$S = \frac{m_3}{\sigma^3}, \ m_3 = \frac{1}{N} \sum_{n=1}^{N} (x[n] - m)^3 \tag{3}$$

The signal output of the first detector in the frequency domain for annular regime (void = 5%) is shown in Figure 6.
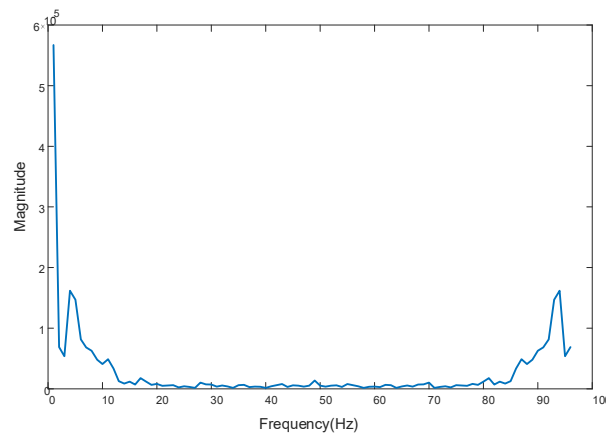

Figure 6. The output signal of the first detector in the frequency domain (annular regime, void fraction = 5%).

As observed in Figure 7, in all the three flow regimes there is a definite link between the air percentages in the pipe and the amplitude of dominant frequency.

The diagram of extracted features in the first detector versus the second detector are shown in Figure 8, which shows the ability of separation for every feature.

As shown in Figure 8, the classification procedure of flow regimes is possible only with one feature (standard deviation), and the three other extracted features are not capable of classifying the mentioned flow regimes due to overlap in their diagrams. According to the obtained results, it can be concluded that the standard deviation is the best feature. Also, the indicated points in each graph show the different void fraction percentages.
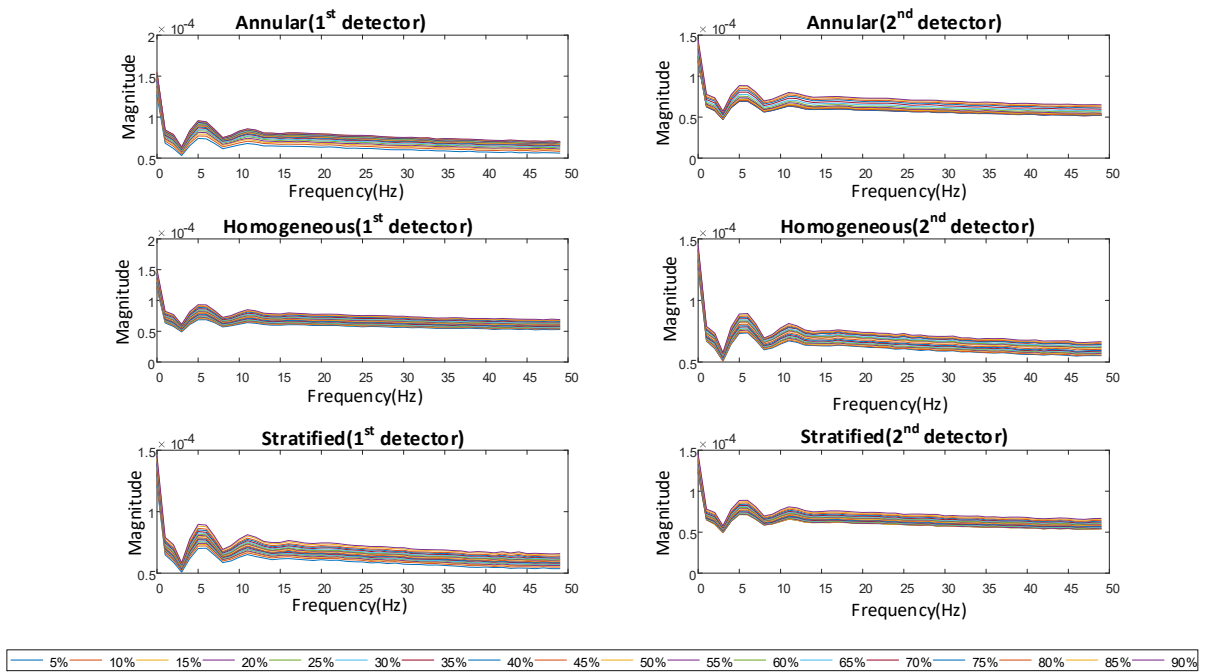
Figure 7. A comparison of fast Fourier transforms of the three flow regimes' signals for various air percentages in the pipe.
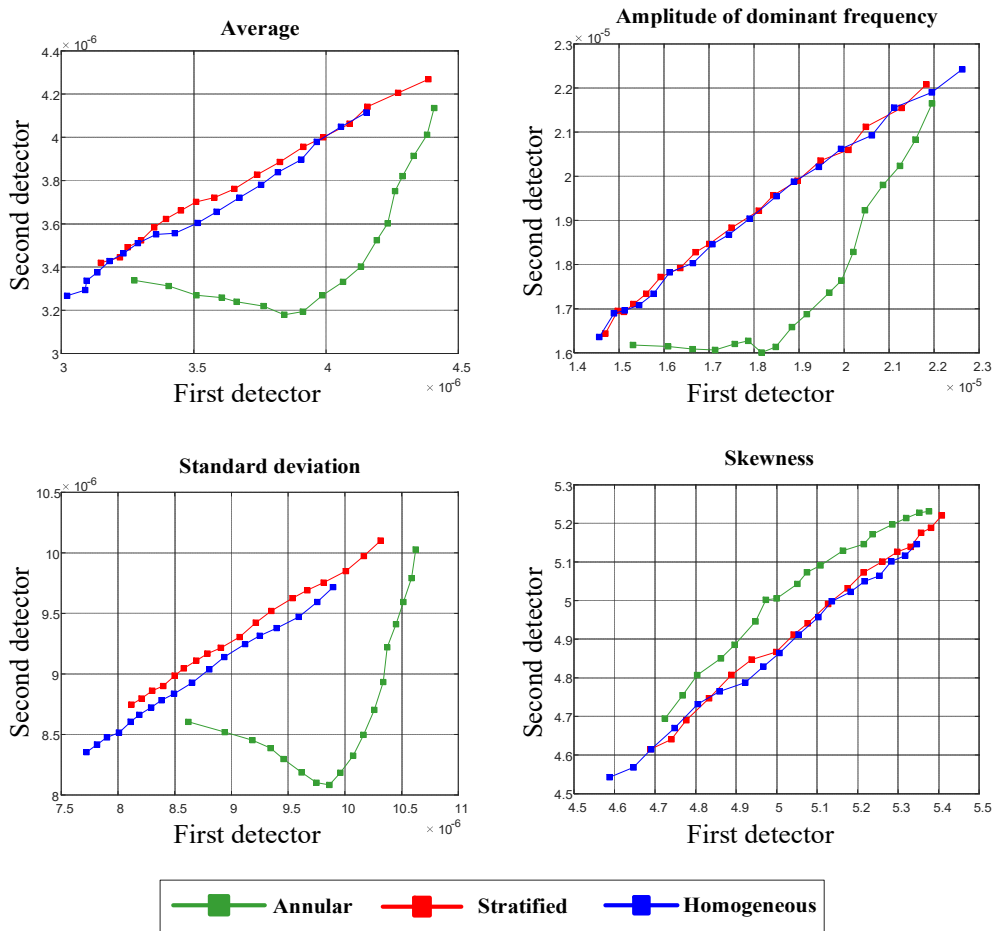

Figure 8. The extracted features from both detectors.

4. Artificial Neural Network

In recent years, different mathematical approaches have been used for analyzing data in many engineering fields [20–39], but it has been proven that the Artificial Neural network (ANN) is the most well-known and powerful tool for prediction and classification. ANNs can be expressed as a mathematical system which consists of several neurons performing in a parallel way, produced in either one or several layers [40,41]. These networks were inspired by biological neural networks [42,43]. Multilayer perceptron (MLP) is a common type of neural network [44,45]. ANN is a suitable technique which is applied for handling the models and classification, as well as prediction [46–59].

In this research, two exclusive networks were adopted for classifying the considered flow regimes and predicting volumetric percentages. Standard deviation of both detectors' frequency spectra was utilized as the implemented ANN inputs, and the output was selected as the flow regime. Numerous ANNs with multiple numbers of neurons and hidden layers were tested and, ultimately, the optimal network was obtained. Figure 9 shows the flowchart of the proposed network to achieve an optimum network with the minimum error ratio.
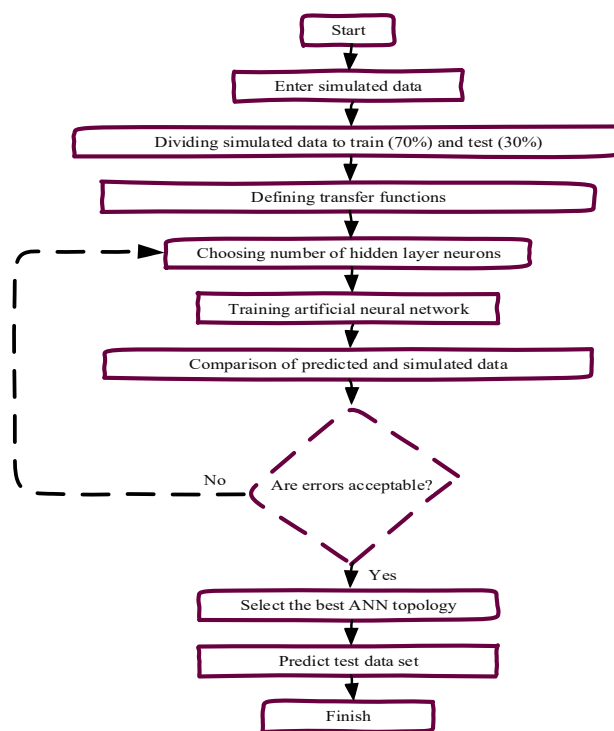
Figure 9. A flowchart for implementing the proposed model.

The parameters and architecture of the obtained network for regime classification are indicated in Table 1 and Figure 10, respectively.

Table 1. The parameters of the adopted neural network in the case of regime classification.

Input Layer	2 Neurons
First hidden layer	4 neurons
Output layer	1 neuron
Epoch numbers	250
Activation function	Tansig

The performance of the employed network for the training and testing processes for regime classification are illustrated in Figure 11.
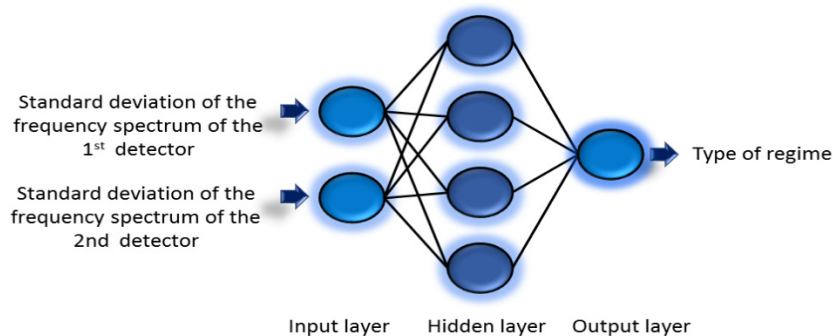
Figure 10. A neural network structure for identifying the flow regimes.

As indicated in Figure 11, in terms of the presented technique, the three flow regimes were classified accurately. The dataset was divided into 70% (39 data samples) and 30% (15 data samples) for model training and testing, respectively.

Figure 11. The performance of implemented ANN for regime classification (training and testing data samples).

The optimum network characteristics and architecture which were employed for void fraction measurement are demonstrated in Table 2 and Figure 12.

Table 2. The neural network parameters utilized for void fraction measurement.

Input Layer	2 Neurons
First hidden layer	3 neurons
Second hidden layer	3 neurons
Output layer	1 neuron
Epoch numbers	250
Activation function	Tansig

Figure 12. The architecture of the adopted network for void fraction prediction.

The network performances for void fraction measurement for training and testing data samples are indicated in Figures 13 and 14, respectively.
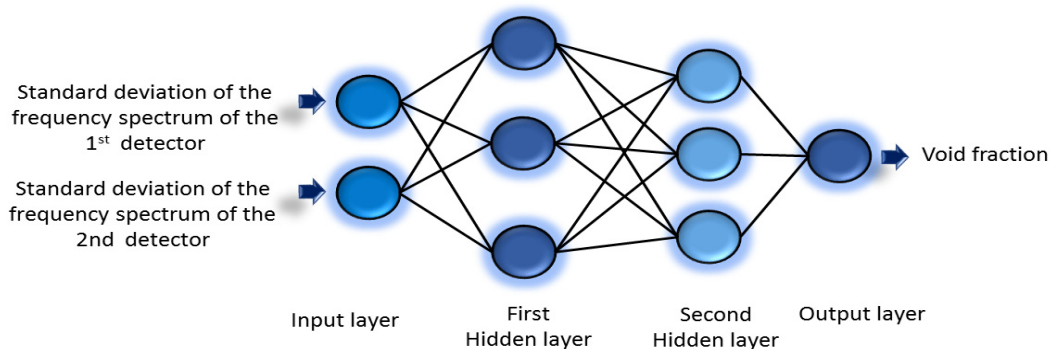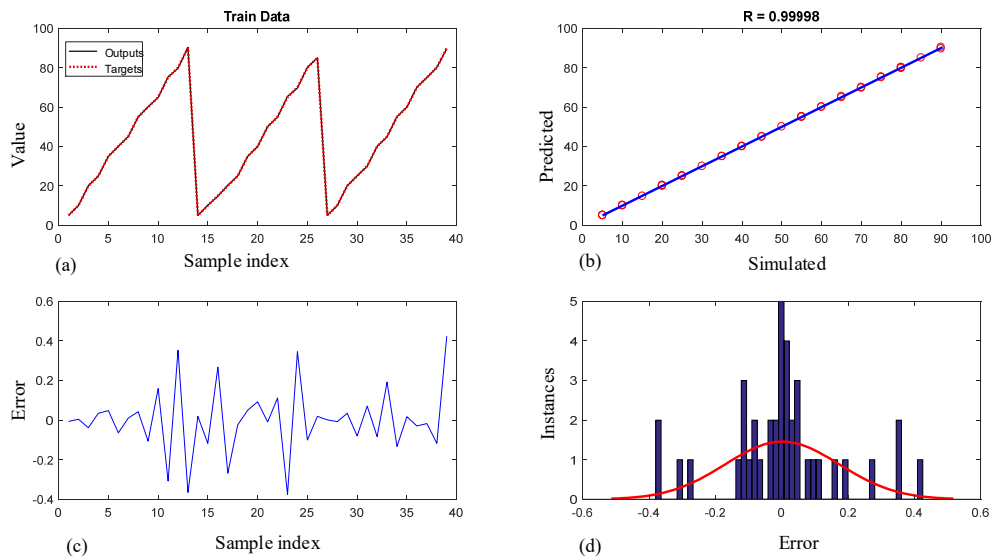

Figure 13. Outcomes of the training process for void fraction measurement: (**a**) fitting, (**b**) regression, (**c**) error, (**d**) error histogram diagram.
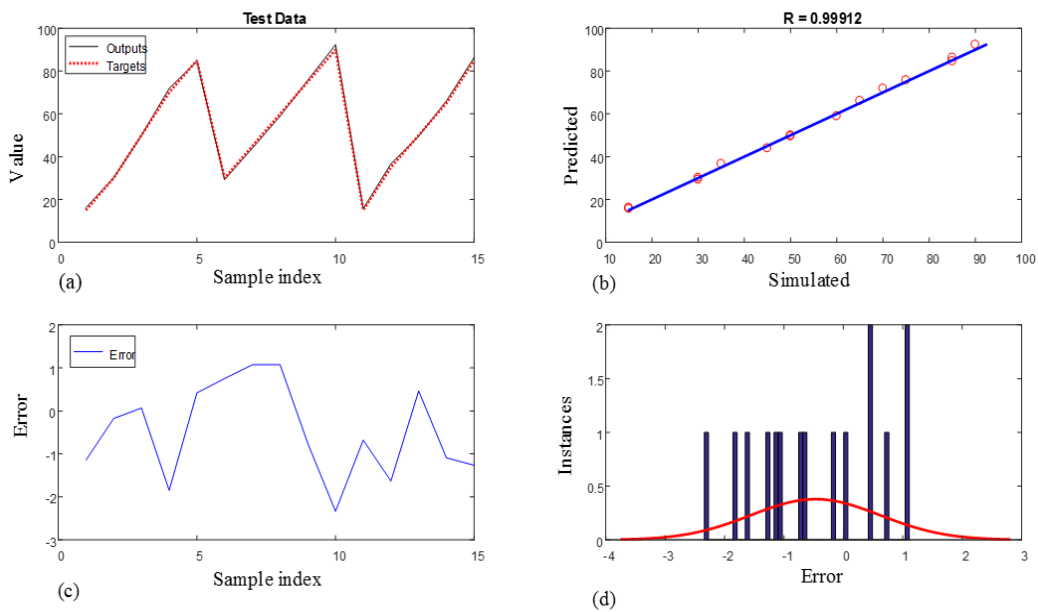
Figure 14. Outcomes of the testing process for void fraction measurement: (**a**) fitting, (**b**) regression, (**c**) error, (**d**) error histogram diagram.

To evaluate the Adopted ANN, the root mean square error percentage (RMSE %) and coefficient of determination (R-squared) were computed by Equations (4) and (5), respectively. The errors achieved are indicated in Table 3.

$$RMSE = \sqrt{\frac{1}{N}\sum_{j=1}^{N}\left[\left(X_j(Sim) - X_j(Pred)\right)\right]^2} \tag{4}$$

$$R^2 = 1 - \frac{\sum_{j=1}^{N}\left(X_j(Sim) - X_j(Pred)\right)^2}{\sum_{j=1}^{N}\left(X_j(Sim) - \overline{X}_j(Sim)\right)^2}, \ \overline{X}_j(Sim) = \frac{1}{N}\sum_{j=1}^{N}X_j(Sim) \tag{5}$$

where *N* is the number of data, *X (sim)* and *X (pred)* stands for simulated and predicted values by neural network, respectively.

Table 3. Computed errors for the training and testing processes.

Data	RMSE %	R^2
Training	0.8697	0.9999
Testing	1.1527	0.9991

A comparison between this study and several research items in this field can be found in Table 4.

Table 4. A comparison between error ratios.

Refs.	Technique	Predicted Volume Fractions (RMSE)
[8] Nazemi et al.	Total count	2.12
[15] Sattari et al.	Time-domain	5.32
[17] Hosseini et al.	Wavelet feature extraction	1.92
Current research	**Frequency-domain**	**1.1527**

Comparisons of simulated and estimated volumetric percentages by ANN for training and testing data sets are indicated in Tables 5 and 6, respectively.

Table 5. A comparison of the actual and predicted values of volumetric percentages (training process).

Data Number	Flow Regime	Volume Fraction Percentages (Actual Values)	Void Fraction Percentages (Predicted by ANN)	Absolute Error between Simulated and Predicted Void Fractions
1	Annular	5	5.00	0.00
2	Annular	10	9.99	0.00
3	Annular	20	20.03	0.03
4	Annular	25	24.96	0.03
5	Annular	35	34.95	0.04
6	Annular	40	40.06	0.06
7	Annular	45	44.99	0.00
8	Annular	55	54.95	0.04
9	Annular	60	60.10	0.10
10	Annular	65	64.84	0.15
11	Annular	75	75.30	0.30
12	Annular	80	79.64	0.35
13	Annular	90	90.36	0.36
14	Stratified	5	4.98	0.01
15	Stratified	10	10.11	0.11
16	Stratified	15	14.73	0.26
17	Stratified	20	20.26	0.26
18	Stratified	25	25.02	0.02
19	Stratified	35	34.95	0.04
20	Stratified	40	39.90	0.09
21	Stratified	50	50.00	0.00
22	Stratified	55	54.88	0.11
23	Stratified	65	65.37	0.37
24	Stratified	70	69.65	0.34
25	Stratified	80	80.10	0.10
26	Stratified	85	84.98	0.01
27	Homogenous	5	4.99	0.00
28	Homogenous	10	10.00	0.00
29	Homogenous	20	19.96	0.03
30	Homogenous	25	25.07	0.07
31	Homogenous	30	29.92	0.07
32	Homogenous	40	40.08	0.08
33	Homogenous	45	44.80	0.19
34	Homogenous	55	55.13	0.13
35	Homogenous	60	59.98	0.01
36	Homogenous	70	70.02	0.02
37	Homogenous	75	75.01	0.01
38	Homogenous	80	80.11	0.11
39	Homogenous	90	89.57	0.42

Table 6. The actual and predicted values of volumetric percentages (testing process).

Data Number	Flow Regime	Volume Fraction Percentages (Actual Values)	Void Fraction Percentages (Predicted by ANN)	Absolute Error between Simulated and Predicted Void Fractions
1	Annular	15	14.91	0.09
2	Annular	30	30.63	0.63
3	Annular	50	48.84	1.16
4	Annular	70	71.65	1.65
5	Annular	85	83.28	1.72
6	Stratified	30	27.47	2.53
7	Stratified	45	45.94	0.94
8	Stratified	60	56.04	3.96
9	Stratified	75	76.94	1.94
10	Stratified	90	86.41	3.59
11	Homogenous	15	13.60	1.40
12	Homogenous	35	35.07	0.07
13	Homogenous	50	52.65	2.65
14	Homogenous	65	64.09	0.91
15	Homogenous	85	83.46	1.54

5. Conclusions

This study proposed the use of fast Fourier transform (FFT) to transform and analyze the frequency domain signals of three flow regimes simulated using MCNP code. The same attributes were extracted in the frequency domain and the standard deviation was recognized as the best feature for determining the flow regimes. Furthermore, two specific neural networks were employed for regime classification and void fraction measurement. Moreover, by using the feature extraction technique and applying neural networks, flow regimes were accurately classified, leading to void fraction percentages with a low root mean square error of 1.1%, which is indicative of the utility of the proposed model.

Institutional Review Board Statement: Not applicable.

Informed Consent Statement: Not applicable.

Data Availability Statement: Not applicable.

Conflicts of Interest: The authors declare no conflict of interest.

References

1. Nazemi, E.; Roshani, G.H.; Feghhi, S.A.H.; Setayeshi, S.; Zadeh, E.E.; Fatehi, A. Optimization of a method for identifying the flow regime and measuring void fraction in a broad beam gamma-ray attenuation technique. *Int. J. Hydrogen Energy* **2016**, *41*, 7438–7444. [CrossRef]
2. Roshani, G.; Nazemi, E.; Feghhi, S. Investigation of using 60 Co source and one detector for determining the flow regime and void fraction in gas–liquid two-phase flows. *Flow Meas. Instrum.* **2016**, *50*, 73–79. [CrossRef]
3. Hanus, R.; Zych, M.; Petryka, L.; Jaszczur, M.; Hanus, P. Signals features extraction in liquid-gas flow measurements using gamma densitometry. Part 1: Time domain. In *EPJ Web of Conferences*; EDP Sciences: Ulys, France, 2016; Volume 114, p. 02035.

4. Alamoudi, M.; Sattari, M.A.; Balubaid, M.; Eftekhari-Zadeh, E.; Nazemi, E.; Taylan, O.; Kalmoun, E.M. Application of Gamma Attenuation Technique and Artificial Intelligence to Detect Scale Thickness in Pipelines in Which Two-Phase Flows with Different Flow Regimes and Void Fractions Exist. *Symmetry* **2021**, *13*, 1198. [CrossRef]

5. Åbro, E.; Johansen, G.A. Improved void fraction determination by means of multibeam gamma-ray attenuation measurements. *Flow Meas. Instrum.* **1999**, *10*, 99–108. [CrossRef]

6. Jing, C.G.; Bai, Q. Flow regime identification of gas/liquid two phase flow in vertical pipe using RBF neural networks. In Proceedings of the Chinese Control and Decision Conference (CCDC), Guilin, China, 17–19 June 2009.

7. Faghihi, R.; Nematollahi, M.; Erfaninia, A.; Adineh, M. Void fraction measurement in modeled two-phase flow inside a vertical pipe by using polyethylene phantoms. *Int. J. Hydrogen Energy* **2015**, *40*, 15206–15212. [CrossRef]

8. Nazemi, E.; Feghhi, S.A.H.; Roshani, G.H.; Peyvandi, R.G.; Setayeshi, S. Precise Void Fraction Measurement in Two-phase Flows Independent of the Flow Regime Using Gamma-ray Attenuation. *Nucl. Eng. Technol.* **2016**, *48*, 64–71. [CrossRef]

9. Nazemi, E.; Feghhi, S.A.H.; Roshani, G.H.; Setayeshi, S.; Peyvandi, R.G. A radiation-based hydrocarbon two-phase flow meter for estimating of phase fraction independent of liquid phase density in stratified regime. *Flow Meas. Instrum.* **2015**, *46*, 25–32. [CrossRef]

10. Roshani, G.H.; Muhammad Ali, P.J.; Mohammed, S.; Hanus, R.; Abdulkareem, L.; Alanezi, A.A.; Nazemi, E.; Eftek-hari-Zadeh, E.; Kalmoun, E.M. Feasibility Study of Using X-ray Tube and GMDH for Measuring Volume Fractions of Annu-lar and Stratified Regimes in Three-Phase Flows. *Symmetry* **2021**, *13*, 613. [CrossRef]

11. Salgado, W.L.; Dam, R.S.; Teixeira, T.P.; Conti, C.C.; Salgado, C.M. Application of artificial intelligence in scale thickness prediction on offshore petroleum using a gamma-ray densitometer. *Radiat. Phys. Chem.* **2020**, *168*, 108549. [CrossRef]

12. Salgado, C.M.; Brandao, L.E.; Schirru, R.; Pereira, C.M.; da Silva, A.X.; Ramos, R. Prediction of volume fractions in three-phase flows using nuclear technique and artificial neural network. *Appl. Radiat. Isot.* **2009**, *67*, 1812–1818. [CrossRef]

13. Salgado, C.M.; Dam, R.S.F.; Salgado, W.L.; Werneck, R.R.A.; Pereira, C.M.N.A.; Schirru, R. The comparison of different multilayer perceptron and General Regression Neural Networks for volume fraction prediction using MCNPX code. *Appl. Radiat. Isot.* **2020**, *162*, 109170. [CrossRef] [PubMed]

14. de Freitas Dam, R.S.; Salgado, W.L.; Affonso, R.R.W.; Schirru, R.; Salgado, C.M. Optimization of radioactive particle tracking methodology in a single-phase flow using MCNP6 code and artificial intelligence methods. *Flow Meas. Instrum.* **2020**, *78*, 101862.

15. Sattari, M.A.; Roshani, G.H.; Hanus, R.; Nazemi, E. Applicability of time-domain feature extraction methods and artificial intelligence in two-phase flow meters based on gamma-ray absorption technique. *Measurement* **2021**, *168*, 108474. [CrossRef]

16. Roshani, M.; Phan, G.; Roshani, G.H.; Hanus, R.; Nazemi, B.; Corniani, E.; Nazemi, E. Combination of X-ray tube and GMDH neural network as a nondestructive and potential technique for measuring characteristics of gas-oil–water three phase flows. *Measurement* **2021**, *168*, 108427. [CrossRef]

17. Hosseini, S.; Taylan, O.; Abusurrah, M.; Akilan, T.; Nazemi, E.; Eftekhari-Zadeh, E.; Bano, F.; Roshani, G.H. Application of Wavelet Feature Extraction and Artificial Neural Networks for Improving the Performance of Gas–Liquid Two-phase Flow Meters Used in Oil and Petrochemical Industries. *Polymers* **2021**, *13*, 3647. [CrossRef]

18. Roshani, M.; Phan, G.; Faraj, R.H.; Phan, N.H.; Roshani, G.H.; Nazemi, B.; Corniani, E.; Nazemi, E. Proposing a gamma radiation based intelligent system for simultaneous analyzing and detecting type and amount of petroleum by-products. *Nucl. Eng. Technol.* **2020**, *53*, 1277–1283. [CrossRef]

19. Phinyomark, A.; Limsakul, C.; Phukpattaranont, P. EMG feature extraction for tolerance of white Gaussian noise. In Proceedings of the International Workshop and Symposium Science Technology, Nong Khai, Thailand, 15–16 December 2008; pp. 178–183.

20. Lalbakhsh, A.; Mohamadpour, G.; Roshani, S.; Ami, M.; Roshani, S.; Sayem, A.S.; Alibakhshikenari, M.; Koziel, S. Design of a compact planar transmission line for miniaturized rat-race coupler with harmonics suppression. *IEEE Access* **2021**, *9*, 129207–129217. [CrossRef]

21. Roshani, S.; Roshani, S. A compact coupler design using meandered line compact microstrip resonant cell (MLCMRC) and bended lines. *Wirel. Netw.* **2021**, *27*, 677–684. [CrossRef]

22. Shukla, N.K.; Mayet, A.M.; Vats, A.; Aggarwal, M.; Raja, R.K.; Verma, R.; Muqeet, M.A. High speed integrated RF–VLC data communication system: Performance constraints and capacity considerations. *Phys. Commun.* **2021**, *50*, 101492. [CrossRef]

23. Hookari, M.; Roshani, S.; Roshani, S. High-efficiency balanced power amplifier using miniaturized harmonics suppressed coupler. *Int. J. RF Microw. Comput.-Aided Eng.* **2020**, *30*, e22252. [CrossRef]

24. Mayet, A.M.; Hussain, A.M.; Hussain, M.M. Three-terminal nanoelectromechanical switch based on tungsten nitride—an amorphous metallic material. *Nanotechnology* **2015**, *27*, 035202. [CrossRef] [PubMed]

25. Lotfi, S.; Roshani, S.; Roshani, S.; Gilan, M.S. Wilkinson power divider with band-pass filtering response and harmonics suppression using open and short stubs. *Frequenz* **2020**, *74*, 169–176. [CrossRef]

26. Mayet, A.; Hussain, M.M. Amorphous WNx Metal for Accelerometers and Gyroscope. In Proceedings of the MRS Fall Meeting 2014, Boston, MA, USA, 30 November–5 December 2014.

27. Jamshidi, M.; Siahkamari, H.; Roshani, S.; Roshani, S. A compact Gysel power divider design using U-shaped and T-shaped resonators with harmonics suppression. *Electromagnetics* **2019**, *39*, 491–504. [CrossRef]

28. Mayet, C.; Smith, E.; Hussain, M.M. Energy reversible switching from amorphous metal based nanoelectromechanical switch, in Nanotechnology (IEEE-NANO). In Proceedings of the 13th IEEE Conference, Vietri sul Mare, Italy, 5–8 August 2013; pp. 366–369.

29. Roshani, S.; Roshani, S. Two-section impedance transformer design and modeling for power amplifier applications. *Appl. Comput. Electromagn. Soc. J.* **2017**, *32*, 1042–1047.

30. Khaibullina, K.S.; Sagirova, L.R.; Sandyga, M.S. Substantiation and selection of an inhibitor for preventing the formation of asphalt-resin-paraffin deposits. Substanciação e seleção de um inibidor para evitar a formação de depósitos de asfalto-resina-parafina. *Period. Tche Quim.* **2020**, *17*, 541–551.

31. Jamshidi, M.B.; Roshani, S.; Talla, J.; Roshani, S.; Peroutka, Z. Size reduction and performance improvement of a microstrip Wilkinson power divider using a hybrid design technique. *Sci. Rep.* **2021**, *11*, 7773. [CrossRef]

32. Mayet, A.; Smith, C.; Hussain, M.M. Amorphous metal based nanoelectromechanical switch. In Proceedings of the 2013 Saudi International Electronics, Communications and Photonics Conference, Riyadh, Saudi Arabia, 27–30 April 2013; pp. 1–5.

33. Hookari, M.; Roshani, S.; Roshani, S. Design of a low pass filter using rhombus-shaped resonators with an analytical LC equivalent circuit. *Turk. J. Electr. Eng. Comput. Sci.* **2020**, *28*, 865–874. [CrossRef]

34. Khaibullina, K.S.; Korobov, G.Y.; Lekomtsev, A.V. Development of an asphalt-resin-paraffin deposits inhibitor and substantiation of the technological parameters of its injection into the bottom-hole formation zone. Desenvolvimento de um inibidor de depósito de asfalto-resinaparafina e subscantiação dos parâmetros tecnológicos de sua injeção na zona de formação de furo inferior. *Period. Tche Quim.* **2020**, *17*, 769–781.

35. Pirasteh, A.; Roshani, S.; Roshani, S. Design of a miniaturized class F power amplifier using capacitor loaded transmission lines. *Frequenz* **2020**, *74*, 145–152. [CrossRef]

36. Tikhomirova, E.A.; Sagirova, L.R.; Khaibullina, K.S. A review on methods of oil saturation modelling using IRAP RMS. *IOP Conf. Ser. Earth Environ. Sci.* **2019**, *378*, 012075. [CrossRef]

37. Roshani, S.; Dehghani, K.; Roshani, S. A lowpass filter design using curved and fountain shaped resonators. *Frequenz* **2019**, *73*, 267–272. [CrossRef]

38. Khaibullina, K. Technology to remove asphaltene, resin and paraffin deposits in wells using organic solvents. In Proceedings of the SPE Annual Technical Conference and Exhibition, Dubai, Saudi Arabia, 26 September 2016. [CrossRef]

39. Roshani, S.; Roshani, S. Design of a compact LPF and a miniaturized Wilkinson power divider using aperiodic stubs with harmonic suppression for wireless applications. *Wirel. Netw.* **2020**, *26*, 1493–1501. [CrossRef]

40. Xie, T.; Ghiaasiaan, S.M.; Karrila, S. Artificial neural network approach for flow regime classification in gass-liquid-fiber flows based on frequency domain analysis of pressure signal. *Chem. Eng. Sci.* **2004**, *59*, 2241–2251. [CrossRef]

41. Hanus, R.; Zych, M.; Kusy, M.; Jaszczur, M.; Petryka, L. Identification of liquid-gas flow regime in a pipeline using gamma-ray absorption technique and computational intelligence methods. *Flow Meas. Instrum.* **2018**, *60*, 17–23. [CrossRef]

42. Roshani, G.H.; Feghhi, S.A.H.; Mahmoudi-Aznaveh, A.; Nazemi, E.; Adineh-Vand, A. Precise volume fraction prediction in oil–water–gas multiphase flows by means of gamma-ray attenuation and artificial neural networks using one detector. *Measurement* **2014**, *51*, 34–41. [CrossRef]

43. Hosseini, S.; Roshani, G.; Setayeshi, S. Precise gamma based two-phase flow meter using frequency feature extraction and only one detector. *Flow Meas. Instrum.* **2020**, *72*, 101693. [CrossRef]

44. Bahiraei, M.; Mazaheri, N.; Hosseini, S. Neural network modeling of thermo-hydraulic attributes and entropy generation of an ecofriendly nanofluid flow inside tubes equipped with novel rotary coaxial double-twisted tape. *Powder Technol.* **2020**, *369*, 162–175. [CrossRef]

45. Tingting, Y.; Junqian, W.; Lintai, W.; Yong, X. Three-stage network for age estimation. *CAAI Trans. Intell. Technol.* **2019**, *4*, 122–126. [CrossRef]

46. Ding, R.; Dai, L.; Li, G.; Liu, H. TDD-net: A tiny defect detection network for printed circuit boards. *CAAI Trans. Intell. Technol.* **2019**, *4*, 110–116. [CrossRef]

47. Salgado, C.; Brandão, L.; Conti, C.; Salgado, W. Density prediction for petroleum and derivatives by gamma-ray attenuation and artificial neural networks. *Appl. Radiat. Isot.* **2016**, *116*, 143–149. [CrossRef]

48. Bahiraei, M.; Foong, L.K.; Hosseini, S.; Mazaheri, N. Predicting heat transfer rate of a ribbed triple-tube heat exchanger working with nanofluid using neural network enhanced by advanced optimization algorithms. *Powder Technol.* **2020**, *381*, 459–476. [CrossRef]

49. Bahiraei, M.; Foong, L.K.; Hosseini, S.; Mazaheri, N. Neural network combined with nature-inspired algorithms to estimate overall heat transfer coefficient of a ribbed triple-tube heat exchanger operating with a hybrid nanofluid. *Measurement* **2021**, *174*, 108967. [CrossRef]

50. Rad, M.Y.; Shahbandegan, S. An Intelligent Algorithm for Mapping of Applications on Parallel Reconfigurable Systems. In Proceedings of the 2020 6th Iranian Conference on Signal Processing and Intelligent Systems (ICSPIS), Sadjad, Iran, 23 December 2020; pp. 1–6.

51. Mayet, A.M.; Salama, A.S.; Alizadeh, S.M.; Nesic, S.; Guerrero, J.W.G.; Eftekhari-Zadeh, E.; Nazemi, E.; Iliyasu, A.M. Applying Data Mining and Artificial Intelligence Techniques for High Precision Measuring of the Two-Phase Flow's Characteristics Independent of the Pipe's Scale Layer. *Electronics* **2022**, *11*, 459. [CrossRef]

52. Eftekhari-Zadeh, E.; Bensalama, A.S.; Roshani, G.H.; Salama, A.S.; Spielmann, C.; Iliyasu, A.M. Enhanced Gamma-Ray Attenuation-Based Detection System Using an Artificial Neural Network. *Photonics* **2022**, *9*, 382. [CrossRef]

53. Hosseini, S.; Setayeshi, S.; Roshani, G.H.; Zahedi, A.; Shama, F. Increasing efficiency of two-phase flowmeters using frequency feature extraction and neural network in detector output spectrum. *J. Model. Eng.* **2021**, *19*, 47–57.

54. Mayet, A.M.; Alizadeh, S.M.; Kakarash, Z.A.; Al-Qahtani, A.A.; Alanazi, A.K.; Alhashimi, H.H.; Eftekhari-Zadeh, E.; Nazemi, E. Introducing a Precise System for Determining Volume Percentages Independent of Scale Thickness and Type of Flow Regime. *Mathematics* **2022**, *10*, 1770. [CrossRef]
55. Roshani, S.; Jamshidi, M.B.; Mohebi, F.; Roshani, S. Design and modeling of a compact power divider with squared resonators using artificial intelligence. *Wirel. Pers. Commun.* **2021**, *117*, 2085–2096. [CrossRef]
56. Mayet, A.M.; Alizadeh, S.M.; Nurgalieva, K.S.; Hanus, R.; Nazemi, E.; Narozhnyy, I.M. Extraction of Time-Domain Characteristics and Selection of Effective Features Using Correlation Analysis to Increase the Accuracy of Petroleum Fluid Monitoring Systems. *Energies* **2022**, *15*, 1986. [CrossRef]
57. Roshani, S.; Azizian, J.; Roshani, S.; Jamshidi, M.; Parandin, F. Design of a miniaturized branch line microstrip coupler with a simple structure using artificial neural network. *Frequenz* **2022**, *76*, 255–263. [CrossRef]
58. Alanazi, A.K.; Alizadeh, S.M.; Nurgalieva, K.S.; Nesic, S.; Grimaldo Guerrero, J.W.; Abo-Dief, H.M.; Eftekhari-Zadeh, E.; Nazemi, E.; Narozhnyy, I.M. Application of Neural Network and Time-Domain Feature Extraction Techniques for Determining Volumetric Percentages and the Type of Two Phase Flow Regimes Independent of Scale Layer Thickness. *Appl. Sci.* **2022**, *12*, 1336. [CrossRef]
59. Roshani, G.; Hanus, R.; Khazaei, A.; Zych, M.; Nazemi, E.; Mosorov, V. Density and velocity determination for single-phase flow based on radiotracer technique and neural networks. *Flow Meas. Instrum.* **2018**, *61*, 9–14. [CrossRef]